Turk J Elec Engin, VOL.13, NO.2 2005, © TÜBİTAK

A Robustness Analysis Procedure for Realistic Missiles

Reşat Özgür DORUK[1], Erol KOCAOĞLAN[2]
[1] *TÜBİTAK – SAGE GKL Middle East Technical University*
06531, Ankara-TURKEY
[2] *Electrical and Electronic Engineering Department, Middle East Technical University*
06531, Ankara-TURKEY
e-mail: e108992@metu.edu.tr

Abstract

This paper presents a robustness analysis procedure for short range realistic missile autopilots. The sensitivity of the autopilots to the aerodynamic parameter uncertainties is investigated through the structured singular value theory where the results are verified through nonlinear simulations. Different types of perturbations are implemented in order to measure the complete performance of the missile.

1. Introduction

The developing technology brings many innovations to the missile guidance and control field. Standard techniques [1, 2, 3, and 4] are available for developing an automated design task. The designs are based on standard models [5, 6, 7, and 8] where the system parameters are taken to be at nominal values. However, in the real environment there are many uncertainties which cause the aerodynamics to be deviated from nominal conditions. This is an important restriction in the design process because of the stability issues. [9, 10] presents the structured singular value theory which can be used to analyze the stability of linear systems in presence of parameter uncertainties. This paper presents the usage of structured singular value theory in missile autopilot designs. In the application, the plant and autopilot designs of [1] are examined. They are designed via the linear quadratic projective control theory [2, 3, and 4] in a systematic way. The structure and framework necessary to analyze those controllers by structured singular value theory are presented and the results are verified through nonlinear simulations.

2. Missile Autopilot Design by Projective Control

2.1. Basic missile modeling

In this research, a canard controlled symmetric missile [1] is used as a plant. For convenience, its nonlinear and linearized models are presented below.

Translational Dynamics:

$$\begin{aligned}\dot{u} &= \tfrac{F_x}{m} - gs\theta + rv - qw \\ \dot{v} &= \tfrac{F_y}{m} + gs\phi c\theta - ru + pw \\ \dot{w} &= \tfrac{F_z}{m} + gc\phi c\theta + qu - pv\end{aligned} \tag{1}$$

Rotational Dynamics:

$$\begin{aligned}\dot{p} &= \tfrac{L}{I_x} \\ \dot{q} &= \tfrac{M}{I_y} + \tfrac{(I_y - I_x)}{I_y} pr \\ \dot{r} &= \tfrac{N}{I_y} + \tfrac{(I_x - I_y)}{I_y} pq\end{aligned} \tag{2}$$

Translational Kinematics:

$$\begin{aligned}\dot{x} &= uc\theta c\psi + v(s\phi s\theta c\psi - c\phi s\psi) + w(s\phi s\theta c\psi + s\phi s\psi) \\ \dot{y} &= uc\theta s\psi + v(s\phi s\theta s\psi + c\phi c\psi) + w(c\phi s\theta s\psi - s\phi c\psi) \\ \dot{z} &= -us\theta + vs\phi c\theta + wc\phi c\theta\end{aligned} \tag{3}$$

Rotational Kinematics:

$$\begin{aligned}\dot{\phi} &= p + qs\phi t\theta + rc\phi t\theta \\ \dot{\theta} &= qc\phi - rs\phi \\ \dot{\psi} &= q\tfrac{s\phi}{c\theta} + r\tfrac{c\phi}{c\theta}\end{aligned} \tag{4}$$

$$\alpha = \tan^{-1}\left(\frac{w}{u}\right), \quad \beta = \sin^{-1}\left(\frac{v}{V}\right) \tag{5}$$

The physical definitions of the state variables mentioned above are:

$[u, v, w]$: The forward, lateral and downward velocities on the body axes of the missile.

$[p, q, r]$: The roll, pitch and yaw angular rates of the missile.

$[x, y, z]$: Position of the missile referenced to the projection of the point where the missile is released from the aircraft on the earth.

$[\phi, \theta, \psi]$: Orientation of the missile (roll, pitch and yaw).

$[\alpha, \beta]$: Angle of attack and sideslip

V : Total velocity

In addition to the 12 state variables presented above there are also accelerations sensed by the body fixed accelerometers which are defined as follows:

$$a_x = \frac{F_x}{m},\ a_y = \frac{F_y}{m},\ a_z = \frac{F_z}{m} \tag{6}$$

2.2. Linear missile model

The linearization of the nonlinear equations of motion in (1), (2), (3) and (4) according to the following assumptions produce the linear pitch and yaw models in (7) and (8).

- The ambient temperature and density is constant.
- Angle of attack, sideslip and fin deflections are small $(\alpha, \beta, \delta < 15^\circ)$.
- Rolling motion is constant and very small $(p, \phi < 5^\circ)$.
- Gravitational acceleration is considered as disturbance.

Pitch Plane State Equations:

$$\begin{pmatrix} \dot{w} \\ \dot{q} \end{pmatrix} = \begin{pmatrix} \left(\frac{Q_d A C_{z_\alpha}}{um}\right) & \left(\frac{Q_d A C_{z_q} d}{2um} + u\right) \\ \left(\frac{Q_d A d C_{m_\alpha}}{u I_y}\right) & \left(\frac{Q_d A d^2}{2u I_y} C_{m_q}\right) \end{pmatrix} \begin{pmatrix} w \\ q \end{pmatrix} + \begin{pmatrix} \left(\frac{Q_d A C_{z_{\delta_e}}}{m}\right) \\ \left(\frac{Q_d A d C_{m_{\delta_e}}}{I_y}\right) \end{pmatrix} \delta_e$$
$$= \begin{pmatrix} \dot{w} \\ \dot{q} \end{pmatrix} = \begin{pmatrix} a_1^p & a_2^p \\ a_3^p & a_4^p \end{pmatrix} \begin{pmatrix} w \\ q \end{pmatrix} + \begin{pmatrix} b_1^p \\ b_2^p \end{pmatrix} \delta_e, \ \mathbf{x} = (w \ \ q)^T, \ u = \delta_e \rightarrow \dot{x} = Ax + Bu \tag{7}$$

Yaw Plane State Equations:

$$\begin{pmatrix} \dot{v} \\ \dot{r} \end{pmatrix} = \begin{pmatrix} \left(\frac{Q_d A C_{y_\beta}}{um}\right) & \left(\frac{Q_d A C_{y_r} d}{2um} - u\right) \\ \left(\frac{Q_d A d C_{n_\beta}}{u I_z}\right) & \left(\frac{Q_d A d^2}{2u I_z} C_{n_r}\right) \end{pmatrix} \begin{pmatrix} v \\ r \end{pmatrix} + \begin{pmatrix} \left(\frac{Q_d A C_{y_{\delta_r}}}{m}\right) \\ \left(\frac{Q_d A d C_{n_{\delta_r}}}{I_z}\right) \end{pmatrix} \delta_r$$
$$= \begin{pmatrix} \dot{v} \\ \dot{r} \end{pmatrix} = \begin{pmatrix} a_1^y & a_2^y \\ a_3^y & a_4^y \end{pmatrix} \begin{pmatrix} v \\ r \end{pmatrix} + \begin{pmatrix} b_1^y \\ b_2^y \end{pmatrix} \delta_r, \ \ \mathbf{x} = (v \ \ r)^T, \ \ u = \delta_r \rightarrow \dot{x} = Ax + Bu \tag{8}$$

In the above models the terms denoted by C_i are called as aerodynamic coefficients and are functions of velocity and altitude. The control surface deflections (δ_e, δ_r) are the effective fin deflections for the missile pitch and yaw motions respectively. Together with the pitch and yaw models, the linearization also produces the linear roll motion equations, as defined below:

$$\begin{pmatrix} \dot{\phi} \\ \dot{p} \end{pmatrix} = \begin{pmatrix} 0 & 1 \\ 0 & \frac{Q_d A d^2 C_{l_p}}{2u I_x} \end{pmatrix} \begin{pmatrix} \phi \\ p \end{pmatrix} + \begin{pmatrix} 0 \\ \frac{Q_d A d C_{l_{\delta_a}}}{I_x} \end{pmatrix} \delta_a$$
$$= \begin{pmatrix} \dot{\phi} \\ \dot{p} \end{pmatrix} = \begin{pmatrix} 0 & 1 \\ 0 & a^r \end{pmatrix} \begin{pmatrix} \phi \\ p \end{pmatrix} + \begin{pmatrix} 0 \\ b^r \end{pmatrix} \delta_a, \ x = (\phi \ \ p)^T, \ u = \delta_a \rightarrow \dot{x} = Ax + Bu \tag{9}$$

The above model is used to design a roll autopilot which regulates the roll rate (p) and angle (ϕ) to zero. This is an important requirement to satisfy the linearization assumptions. The details of the autopilot design are given in [1].

2.3. The actuator

The actuator model given in [1] has two saturation elements: one on angular rate and another on position, respectively. It is a second order nonlinear system which is linearized for structured singular value analysis. As a result of linearization, the basic second order system with natural frequency ω_0 and damping ratio ζ given below is obtained:

$$\frac{\delta_i}{\delta_i^c} = \frac{\omega_o^2}{s^2 + 2\zeta\omega_o s + \omega_o^2} \tag{10}$$

2.4. Missile autopilot design

The analysis will be studied on pitch rate and acceleration autopilots [1] each of which are designed using static and dynamic linear quadratic projective control theories [2, 3, and 4]. The purpose of the projective control is to approximate the full state feedback linear quadratic controller design by feedback from available states (output feedback). For a general state space notation like below,

$$\begin{aligned} \dot{\mathbf{x}} &= \mathbf{A}\mathbf{x} + \mathbf{B}\mathbf{u} \\ \mathbf{y} &= \mathbf{C}\mathbf{x} + \mathbf{D}\mathbf{u} \end{aligned} \tag{11}$$

the linear quadratic design is a feedback gain vector $u = -K_{full}x$,which minimizes the following performance index:

$$J = \int_{-\infty}^{\infty} \left(\mathbf{x}^{\mathbf{T}}\mathbf{Q}\mathbf{x} + \mathbf{u}^{\mathbf{T}}\mathbf{R}\mathbf{u}\right) dt. \tag{12}$$

In missile autopilots the vector $\mathbf{x}$ is, $\begin{pmatrix} w & q & \varepsilon_q \end{pmatrix}$, and for yaw autopilots it is $\begin{pmatrix} v & r & \varepsilon_r \end{pmatrix}$, where $\varepsilon_q = \int (r_q - q)dt$ and $\varepsilon_r = \int (r_r - r)dt$. The couple (v, w) can not be directly measured and thus the full state feedback is not possible. To compensate for this deficiency, [3] and [4] present a cure which retains the dominant eigenvalues of the closed loop spectrum of the full state feedback linear control system. The closed loop spectrum of the full state feedback control system is shown below:

$$\begin{aligned} \mathbf{F}\mathbf{X} &= \mathbf{X}\Lambda \\ \mathbf{F} &= \left(\mathbf{A} - \mathbf{B}\mathbf{K}_{\mathbf{full}}\right). \end{aligned} \tag{13}$$

where $\mathbf{X}$ is the full eigenvector matrix and Λ is the matrix of closed loop eigenvalues along the diagonal. If the dominant eigenvalue matrix is shown by $\Lambda_{\mathbf{r}}$ then the corresponding eigenvector matrix is denoted by $\mathbf{X}_{\mathbf{r}}$ and the spectrum equation is $\mathbf{F}\mathbf{X}_{\mathbf{r}} = \mathbf{X}_{\mathbf{r}}\Lambda_{\mathbf{r}}$. The output feedback gain vector $\mathbf{K}_{\mathbf{pro}}$ is obtained through the projection equation below:

$$\begin{aligned} &\mathbf{P} = \mathbf{X}_{\mathbf{r}} \left(\mathbf{C}_{\mathbf{r}}\mathbf{X}_{\mathbf{r}}\right)^{-1} \mathbf{C}_{\mathbf{r}},\ \hat{\mathbf{y}} = \mathbf{C}_{\mathbf{r}}\mathbf{x} \\ &\mathbf{K}_{\mathbf{pro}} = \mathbf{K}_{\mathbf{full}}\mathbf{P},\ \mathbf{u} = -\mathbf{K}_{\mathbf{pro}}\mathbf{x} \end{aligned} \tag{14}$$

where $\hat{\mathbf{y}}$ is the vector of available states. The closed loop poles are the eigenvalues of $(\mathbf{A}-\mathbf{BK_{pro}})$. Since there is no dynamic compensator in the design, the approach is called as static projective control. If the resultant spectrum is unstable, a compensator of the following form can be proposed:

$$\begin{aligned}\mathbf{u} &= -\mathbf{K_y}\hat{\mathbf{y}} - \mathbf{K_z}\mathbf{z}\\ \dot{\mathbf{z}} &= \mathbf{H_0}\mathbf{z} + \mathbf{D_0}\hat{\mathbf{y}}\end{aligned} \tag{15}$$

where $\mathbf{z}$ is the compensator state. The approach is called as dynamic projective control. The details of the compensator design are presented in [1, 2, 3 and 4].

The augmentation of the linear pitch and yaw models with the integral of the acceleration error will produce the following:

$$\begin{bmatrix}\dot{\varepsilon}_{a_z}\\ \dot{q}\\ \dot{w}\end{bmatrix} = \begin{pmatrix}0 & -a_2^p+u & -a_1^p\\ 0 & a_4^p & a_3^p\\ 0 & a_2^p & a_1^p\end{pmatrix}\begin{bmatrix}\varepsilon_{a_z}\\ q\\ w\end{bmatrix} + \begin{bmatrix}-b_1^p\\ b_2^p\\ b_1^p\end{bmatrix}\delta_e + \begin{bmatrix}1\\ 0\\ 0\end{bmatrix} r_{a_z}$$

$$\dot{\mathbf{x}}^{pac} = \hat{\mathbf{A}}^{pac}\mathbf{x}^{pac} + \hat{\mathbf{B}}^{pac}u^{pac} + \hat{\mathbf{G}}^{pac}r_{a_z},\ \varepsilon_{a_z} = \int (r_{a_z} - a_z)dt$$

$$\mathbf{x}^{pac} = \begin{pmatrix}\varepsilon_{a_z} & q & w\end{pmatrix}^T,\quad u^{pac} = \delta_e$$

$$\begin{bmatrix}\dot{\varepsilon}_{a_y}\\ \dot{r}\\ \dot{v}\end{bmatrix} = \begin{pmatrix}0 & -a_2^y-u & -a_1^y\\ 0 & a_4^y & a_3^y\\ 0 & a_2^y & a_1^y\end{pmatrix}\begin{bmatrix}\varepsilon_{a_y}\\ r\\ v\end{bmatrix} + \begin{bmatrix}-b_1^y\\ b_2^y\\ b_1^y\end{bmatrix}\delta_r + \begin{bmatrix}1\\ 0\\ 0\end{bmatrix} r_{a_y} \tag{16}$$

$$\dot{\mathbf{x}}^{yac} = \hat{\mathbf{A}}^{yac}\mathbf{x}^{yac} + \hat{\mathbf{B}}^{yac}u^{yac} + \hat{\mathbf{G}}^{yac}r_{a_y},\ \varepsilon_{a_y} = \int \left(r_{a_y} - a_y\right)dt$$

$$\mathbf{x}^{yac} = \begin{pmatrix}\varepsilon_{a_y} & r & v\end{pmatrix}^T,\quad u^{yac} = \delta_r$$

whereas the same modification for the rate autopilots will be:

$$\begin{bmatrix}\dot{\varepsilon}_q\\ \dot{q}\\ \dot{w}\end{bmatrix} = \begin{pmatrix}0 & -1 & 0\\ 0 & a_4^p & a_3^p\\ 0 & a_2^p & a_1^p\end{pmatrix}\begin{bmatrix}\varepsilon_q\\ q\\ w\end{bmatrix} + \begin{bmatrix}0\\ b_2^p\\ b_1^p\end{bmatrix}\delta_e + \begin{bmatrix}1\\ 0\\ 0\end{bmatrix} r_q$$

$$\dot{\mathbf{x}}^{prt} = \hat{\mathbf{A}}^{prt}\mathbf{x}^{prt} + \hat{\mathbf{B}}^{prt}u^{prt} + \hat{\mathbf{G}}^{prt}r_q,\ \varepsilon_q = \int (r_q - q)dt$$

$$\mathbf{x}^{prt} = \begin{pmatrix}\varepsilon_q & q & w\end{pmatrix}^T,\quad u^{prt} = \delta_e$$

$$\begin{bmatrix}\dot{\varepsilon}_r\\ \dot{r}\\ \dot{v}\end{bmatrix} = \begin{pmatrix}0 & -1 & 0\\ 0 & a_4^y & a_3^y\\ 0 & a_2^y & a_1^y\end{pmatrix}\begin{bmatrix}\varepsilon_r\\ r\\ v\end{bmatrix} + \begin{bmatrix}0\\ b_2^y\\ b_1^y\end{bmatrix}\delta_r + \begin{bmatrix}1\\ 0\\ 0\end{bmatrix} r_r \tag{17}$$

$$\dot{\mathbf{x}}^{yrt} = \hat{\mathbf{A}}^{yrt}\mathbf{x}^{yrt} + \hat{\mathbf{B}}^{yrt}u^{yrt} + \hat{\mathbf{G}}^{yrt}r_r,\ \varepsilon_r = \int (r_r - r)dt$$

$$\mathbf{x}^{yrt} = \begin{pmatrix}\varepsilon_r & r & v\end{pmatrix}^T,\quad u^{yrt} = \delta_r$$

The linear quadratic design will minimize the following quadratic performance index:

$$J_r = \int_{-\infty}^{\infty} (q_r \varepsilon_{q,r}^2 + \delta_{e,r}^2) dt$$
$$J_a = \int_{-\infty}^{\infty} (q_a \varepsilon_{a_z,a_y}^2 + \delta_{e,r}^2) dt \tag{18}$$

The selection of the quadratic performance index $(q_a,\ q_r)$ is performed according to the selected design criteria that are shown below:

$$\begin{array}{ll} 0.3 < t_s < 0.4 & \\ G.M > 10\,dB & \textit{Rate Autopilots} \\ P.M > 50^\circ & \\ 0.6 < t_s < 0.8 & \\ G.M > 10dB & \textit{Acceleration Autopilots} \\ P.M > 50^\circ & \end{array} \tag{19}$$

For the aerodynamic operating points $V = 0.86\,Mach$, $h = 5000\,m$, the design criteria are satisfied at $q_r = 65$ and $q_a = 2.5$ for rate and acceleration autopilot respectively.

The projective control of the rate autopilots are successful for both static and dynamic cases whereas the acceleration autopilot can only be stabilized using an observer (designed by dynamic projective control). In Figure 1, the diagram of the static rate autopilot is shown.

The controller sections for dynamic rate and acceleration autopilots are presented in Figure 2 and Figure 3, respectively. The static projective rate autopilot gains in Figure 1 at the given aerodynamic operating points are given below:

$$K_h^p = -7.5219$$
$$K_q^p = -0.68415 \tag{20}$$

Similarly, the controller – compensator gains of the dynamic rate and acceleration autopilots are shown in (21).

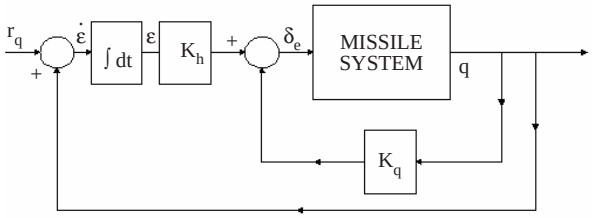

Figure 1. Static projective rate autopilot.

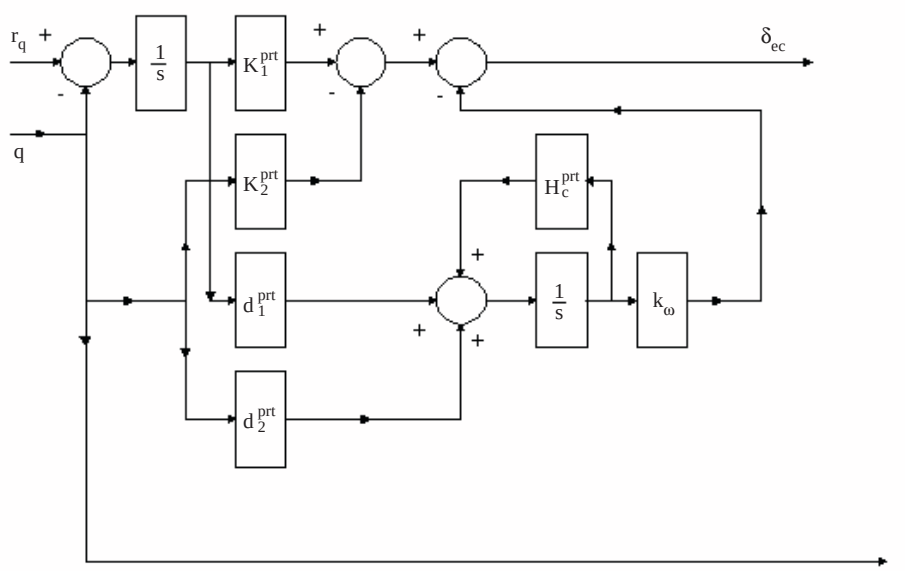

Figure 2. Dynamic projective rate autopilot.

$$
\begin{aligned}
\mathbf{D}_{\mathbf{c}}^{*} &= \begin{pmatrix} d_1^{*} & d_2^{*} \end{pmatrix} \\
\mathbf{K}_{\Theta}^{*} &= \begin{pmatrix} K_1^{*} & K_2^{*} \end{pmatrix} \\
H_c^{prt} &= -0.4746 \\
\mathbf{D}_{\mathbf{c}}^{prt} &= \begin{pmatrix} 2372 & -206.45 \end{pmatrix} \\
\mathbf{K}_{\Theta}^{prt} &= \begin{pmatrix} 7.5219 & -0.70319 \end{pmatrix} \\
K_{\omega}^{prt} &= 0.001894 \\
H_c^{pac} &= -27.535 \\
\mathbf{D}_{\mathbf{c}}^{pac} &= \begin{pmatrix} -99.565 & 63.96 \end{pmatrix} \\
\mathbf{K}_{\Gamma}^{pac} &= \begin{pmatrix} -1.6329 & 0.66699 \end{pmatrix} \\
K_{\xi}^{pac} &= -0.40393
\end{aligned}
\tag{21}
$$

The dynamic projective rate and acceleration autopilots are presented in single block forms for each gain component. The reason for that is to make the development of the dynamic control algorithm easier and to use this autopilot in Linear Fractional Transformation (LFT) methods in the foregoing sections.

3. Structured Singular Value Analyses

The application of the structured singular value (μ) analysis approach to the linear missile model and the autopilot are performed through frameworks developed by the linear fractional transformation (LFT) [9, 10]. In the analysis, the theory presented in [9] is implemented using the MATLAB algorithms of [9, 11, and 12].

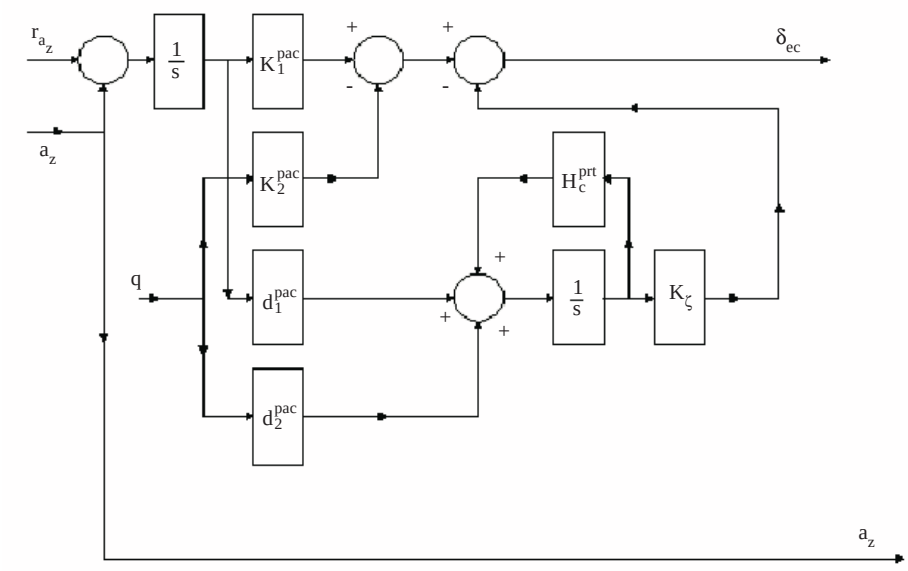

Figure 3. Dynamic projective acceleration autopilot.

3.1. Linear fractional transformations (LFT)

3.1.1. Introduction to linear fractional transformations

To analyze the effects of parameter uncertainties in the closed loop system, a systematic way of uncertainty analysis is developed in [9, 10, 11, 12, 13]. The general form of uncertainty in a linear system parameter c is expressed as $c = \bar{c}(1 + \delta)$ where $\bar{c}$ is the nominal value of the interested parameter. The linear fractional transformation (LFT) separates the nominal and uncertain parts of the parameters to a matrix interconnection as shown in Figure 4.

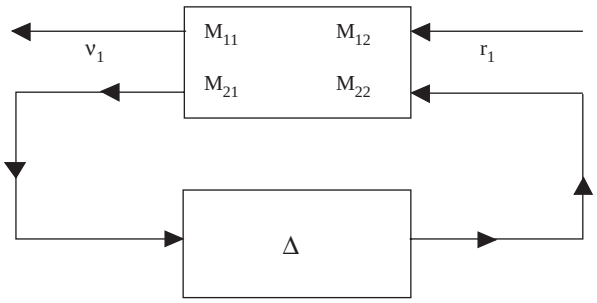

Figure 4. The LFT decomposition of an uncertain system.

The relationship between r_1 and v_1 is expressed by the following:

$$\begin{aligned} \mathbf{v_1} &= (\mathbf{M_{11}} + \mathbf{M_{12}}\Delta(\mathbf{I} - \mathbf{M_{22}}\Delta)^{-1}\mathbf{M_{21}})\mathbf{r_1} \\ \mathbf{v_1} &= \mathbf{F_L}(\mathbf{M}, \Delta)\mathbf{r_1} \\ \mathbf{M} &= \begin{pmatrix} \mathbf{M_{11}} & \mathbf{M_{12}} \\ \mathbf{M_{21}} & \mathbf{M_{22}} \end{pmatrix} \end{aligned} \tag{22}$$

The matrix Δ is the uncertainty matrix and for a single parameter it is the uncertainty δ and $\mathbf{M}$ is the frequency response matrix of the nominal system. For the simple uncertainty $\overline{c}$ the elements of matrix $\mathbf{M}$ will be as shown below:

$$\begin{aligned} &\mathbf{M_{11}} = \bar{c},\ \mathbf{M_{12}} = \bar{c},\ \mathbf{M_{21}} = 1,\ \mathbf{M_{22}} = 0,\ \Delta = \delta \\ &v_1 = cr_1 \end{aligned} \tag{23}$$

For low order systems, the analysis framework can be formed by replacing all uncertainties in its mathematical model by the LFT equivalent in Figure 4. However, if the number of parameters are increased like in the pitch axis linear model in (7), then a state space conversion approach is presented in [13] for application to standard space form like,

$$\begin{aligned} \dot{\hat{\mathbf{x}}} &= \hat{\mathbf{A}}\hat{\mathbf{x}} + \hat{\mathbf{B}}\hat{\mathbf{u}} \\ \hat{\mathbf{y}} &= \hat{\mathbf{C}}\hat{\mathbf{x}} + \hat{\mathbf{D}}\hat{\mathbf{u}} \end{aligned} \tag{24}$$

The above representation can be written in the input – output – state compact form as shown below:

$$\begin{pmatrix} \dot{\hat{\mathbf{x}}} \\ \hat{\mathbf{y}} \end{pmatrix} = \begin{pmatrix} \hat{\mathbf{A}} & \hat{\mathbf{B}} \\ \hat{\mathbf{C}} & \hat{\mathbf{D}} \end{pmatrix} \begin{pmatrix} \hat{\mathbf{x}} \\ \hat{\mathbf{u}} \end{pmatrix} \tag{25}$$

The compact form can now be decomposed to its nominal and perturbed parts as presented below:

$$\begin{pmatrix} \hat{\mathbf{A}} & \hat{\mathbf{B}} \\ \hat{\mathbf{C}} & \hat{\mathbf{D}} \end{pmatrix} = \begin{pmatrix} \bar{\mathbf{A}} & \bar{\mathbf{B}} \\ \bar{\mathbf{C}} & \bar{\mathbf{D}} \end{pmatrix} + \begin{pmatrix} \mathbf{A_1} & \mathbf{B_1} \\ \mathbf{C_1} & \mathbf{D_1} \end{pmatrix} \delta_1 + \begin{pmatrix} \mathbf{A_2} & \mathbf{B_2} \\ \mathbf{C_2} & \mathbf{D_2} \end{pmatrix} \delta_2 + ... + \begin{pmatrix} \mathbf{A}_n & \mathbf{B}_n \\ \mathbf{C}_n & \mathbf{D}_n \end{pmatrix} \delta_n \tag{26}$$

$$\mathbf{E} = \bar{\mathbf{E}} + \mathbf{E_1}\delta_1 + \mathbf{E_2}\delta_2 + ... + \mathbf{E_n}\delta_n$$

where each E_i can be expressed as a product of a column and a row vector like $\mathbf{E_i} = \beta_\mathbf{i}\alpha_\mathbf{i}$ such that,

$$\mathbf{E} = \bar{\mathbf{E}} + \sum_{i=1}^{n} \beta_\mathbf{i}\delta_\mathbf{i}\alpha_\mathbf{i} \tag{27}$$

for n uncertain parameters. Lastly, the elements of the nominal parameter matrix are formed as:

$$\mathbf{A_m} = \bar{\mathbf{E}},\ \mathbf{B_m} = \begin{pmatrix} \beta_1 & \beta_2 & .... & \beta_n \end{pmatrix},\ \mathbf{C_m} = \begin{pmatrix} \alpha_1 \\ \alpha_2 \\ : \\ \alpha_n \end{pmatrix},\ \mathbf{M} = \begin{pmatrix} \mathbf{A_m} & \mathbf{B_m} \\ \mathbf{C_m} & \mathbf{0} \end{pmatrix} \tag{28}$$

3.1.2. LFT Model of the Actuator

If there is a possibility of a deviation in the natural frequency of the actuator in (10) then in order to analyze its effects on stability the LFT model of the actuator in Figure 4 can be used. The uncertainty in natural frequency is expressed as shown below:

$$\omega_0 = \bar{\omega}_0 \, (1 + \delta) \tag{29}$$

In the figure, the nonlinear uncertainty due to ω_0^2 is expressed as $\omega_0^2 = \omega_0 \omega_0$ which result in two LFT connections put in cascaded form. Together with the uncertainty in $2\zeta\omega_0$ in Figure 5a one gets three repeated uncertainties as shown in Figure 5b. They are expressed as a 3×3 diagonal block in the overall uncertainty matrix Δ.

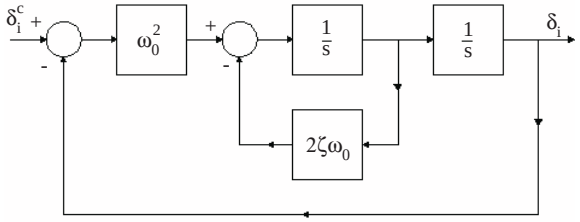

Figure 5a. Standard actuator model.

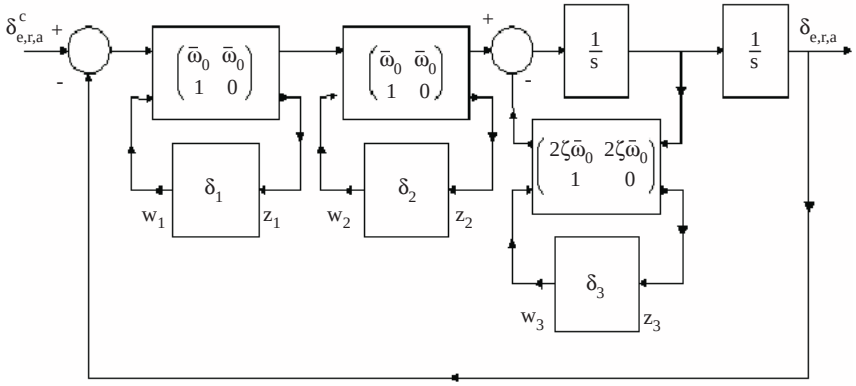

Figure 5b. Actuator LFT model.

3.1.3. LFT of the linear missile model

For the missile model, a matrix expansion method is presented in [13, 14] is used. By this way, the state space representation of the linear missile model is separated into its nominal and uncertain parts. The derivation is given only for the pitch rate autopilot. Similar procedure can be followed for the acceleration autopilot. The corresponding results will be presented after the pitch rate autopilot.

The uncertainties in the aerodynamic coefficients of the missile model (or the entries in (7) are expressed as shown below:

$$\begin{aligned} a_i^j &= \bar{a}_i^j (1 + \delta) \\ b_i^j &= \bar{b}_i^j (1 + \delta) \end{aligned} \tag{30}$$

The procedure of 3.1.1 can be used to convert the system matrices in (7) to the form of (25) considering the pitch rate q as the controlled output, as shown below:

$$\begin{pmatrix} \dot{w} \\ \dot{q} \\ q \end{pmatrix} = \begin{pmatrix} a_1^p & a_2^p & b_1^p \\ a_3^p & a_4^p & b_2^p \\ 0 & 1 & 0 \end{pmatrix} \begin{pmatrix} w \\ q \\ \delta_e \end{pmatrix} \tag{31}$$

According to (26), the above representation can be expanded as:

$$\begin{pmatrix} a_1^p & a_2^p & b_1^p \\ a_3^p & a_4^p & b_2^p \\ 0 & 1 & 0 \end{pmatrix} = \begin{pmatrix} \bar{a}_1^p & \bar{a}_2^p & \bar{b}_1^p \\ \bar{a}_3^p & \bar{a}_4^p & \bar{b}_2^p \\ 0 & 1 & 0 \end{pmatrix} + \begin{pmatrix} \bar{a}_1^p & 0 & 0 \\ 0 & 0 & 0 \\ 0 & 0 & 0 \end{pmatrix} \delta_1 + \begin{pmatrix} 0 & \bar{a}_2^p & 0 \\ 0 & 0 & 0 \\ 0 & 0 & 0 \end{pmatrix} \delta_2 + \begin{pmatrix} 0 & 0 & 0 \\ \bar{a}_3^p & 0 & 0 \\ 0 & 0 & 0 \end{pmatrix} \delta_3 + \begin{pmatrix} 0 & 0 & 0 \\ 0 & \bar{a}_4^p & 0 \\ 0 & 0 & 0 \end{pmatrix} \delta_4 + \begin{pmatrix} 0 & 0 & \bar{b}_1^p \\ 0 & 0 & 0 \\ 0 & 0 & 0 \end{pmatrix} \delta_5 + \begin{pmatrix} 0 & 0 & 0 \\ 0 & 0 & \bar{b}_2^p \\ 0 & 0 & 0 \end{pmatrix} \delta_6 \tag{32}$$

Further processing of the above equation results in:

$$\begin{pmatrix} \bar{a}_1^p & \bar{a}_2^p & \bar{b}_1^p \\ \bar{a}_3^p & \bar{a}_4^p & \bar{b}_2^p \\ 0 & 1 & 0 \end{pmatrix} + \begin{pmatrix} \bar{a}_1^p \\ 0 \\ 0 \end{pmatrix} \begin{pmatrix} 1 & 0 & 0 \end{pmatrix} \delta_1 + \begin{pmatrix} \bar{a}_2^p \\ 0 \\ 0 \end{pmatrix} \begin{pmatrix} 0 & 1 & 0 \end{pmatrix} \delta_2 + \begin{pmatrix} 0 \\ \bar{a}_3^p \\ 0 \end{pmatrix} \begin{pmatrix} 1 & 0 & 0 \end{pmatrix} \delta_3 + \begin{pmatrix} 0 \\ \bar{a}_4^p \\ 0 \end{pmatrix} \begin{pmatrix} 0 & 1 & 0 \end{pmatrix} \delta_4 + \begin{pmatrix} \bar{b}_1^p \\ 0 \\ 0 \end{pmatrix} \begin{pmatrix} 0 & 0 & 1 \end{pmatrix} \delta_5 + \begin{pmatrix} 0 \\ \bar{b}_2^p \\ 0 \end{pmatrix} \begin{pmatrix} 0 & 0 & 1 \end{pmatrix} \delta_6 \tag{33}$$

Finally, recompilation of the matrices in (31) and (33) using the (27) and (28) gives the multi input multi output (MIMO) nominal analysis model which is shown in (34). The inputs w_i correspond to the outputs of the uncertainty matrix Δ in Figure 4, which includes the uncertainty information related to each parameter.

The outputs z_j of the MIMO structure of (34), are the outputs of the nominal part of the parameter according to Figure 4. The mathematical representation of the MIMO model is shown below:

$$\begin{pmatrix} \dot{w} \\ \dot{q} \\ q \\ z_1 \\ z_2 \\ z_3 \\ z_4 \\ z_5 \\ z_6 \end{pmatrix} = \begin{pmatrix} \bar{a}_1^p & \bar{a}_2^p & \bar{b}_1^p & \bar{a}_1^p & \bar{a}_2^p & 0 & 0 & \bar{b}_1^p & 0 \\ \bar{a}_3^p & \bar{a}_4^p & \bar{b}_2^p & 0 & 0 & \bar{a}_3^p & \bar{a}_4^p & 0 & \bar{b}_2^p \\ 0 & 1 & 0 & 0 & 0 & 0 & 0 & 0 & 0 \\ 1 & 0 & 0 & 0 & 0 & 0 & 0 & 0 & 0 \\ 0 & 1 & 0 & 0 & 0 & 0 & 0 & 0 & 0 \\ 1 & 0 & 0 & 0 & 0 & 0 & 0 & 0 & 0 \\ 0 & 1 & 0 & 0 & 0 & 0 & 0 & 0 & 0 \\ 0 & 0 & 1 & 0 & 0 & 0 & 0 & 0 & 0 \\ 0 & 0 & 1 & 0 & 0 & 0 & 0 & 0 & 0 \end{pmatrix} \begin{pmatrix} w \\ q \\ \delta_e \\ w_1 \\ w_2 \\ w_3 \\ w_4 \\ w_5 \\ w_6 \end{pmatrix} \tag{34}$$

Together with the actuator model in Figure 5b, the number of uncertainties adds up to 9. Thus the uncertainty matrix becomes a 9×9 block diagonal structure with one block being in 3×3 diagonal form. In the analysis, controller gains are taken to be deterministic quantities so there is no need of LFT forming for the autopilot. The overall framework for structured singular value analysis of the pitch autopilot can be seen in Figure 6.

By using a similar procedure, the compact form and its decomposition for the dynamic projective acceleration autopilot where the controlled variables (outputs) are pitch rate and acceleration (q and a_z) is presented as shown below:

$$\begin{pmatrix} \dot{w} \\ \dot{q} \\ a_z \\ q \end{pmatrix} = \begin{pmatrix} a_1^p & a_2^p & b_1^p \\ a_3^p & a_4^p & b_2^p \\ a_1^p & a_2^p - u & b_1^p \\ 0 & 1 & 0 \end{pmatrix} \begin{pmatrix} w \\ q \\ \delta_e \end{pmatrix} \tag{35}$$

$$\begin{pmatrix} a_1^p & a_2^p & b_1^p \\ a_3^p & a_4^p & b_2^p \\ a_1^p & a_2^p - u & b_1^p \\ 0 & 1 & 0 \end{pmatrix} = \begin{pmatrix} \bar{a}_1^p & \bar{a}_2^p & \bar{b}_1^p \\ \bar{a}_3^p & \bar{a}_4^p & \bar{b}_2^p \\ \bar{a}_1^p & \bar{a}_2^p - u & \bar{b}_1^p \\ 0 & 1 & 0 \end{pmatrix} + \begin{pmatrix} \bar{a}_1^p & 0 & 0 \\ 0 & 0 & 0 \\ \bar{a}_1^p & 0 & 0 \\ 0 & 0 & 0 \end{pmatrix} \delta_1 + \begin{pmatrix} 0 & \bar{a}_2^p & 0 \\ 0 & 0 & 0 \\ 0 & \bar{a}_2^p & 0 \\ 0 & 0 & 0 \end{pmatrix} \delta_2 + \begin{pmatrix} 0 & 0 & 0 \\ \bar{a}_3^p & 0 & 0 \\ 0 & 0 & 0 \\ 0 & 0 & 0 \end{pmatrix} \delta_3 + \begin{pmatrix} 0 & 0 & 0 \\ 0 & \bar{a}_4^p & 0 \\ 0 & 0 & 0 \\ 0 & 0 & 0 \end{pmatrix} \delta_4 + \begin{pmatrix} 0 & 0 & \bar{b}_1^p \\ 0 & 0 & 0 \\ 0 & 0 & \bar{b}_1^p \\ 0 & 0 & 0 \end{pmatrix} \delta_5 + \begin{pmatrix} 0 & 0 & 0 \\ 0 & 0 & \bar{b}_2^p \\ 0 & 0 & 0 \\ 0 & 0 & 0 \end{pmatrix} \delta_6 \tag{36}$$

The application of (27) and (28) will yield the following:

$$\bar{\mathbf{E}} + \begin{pmatrix} \bar{a}_1^p \\ 0 \\ \bar{a}_1^p \\ 0 \end{pmatrix} \begin{pmatrix} 1 & 0 & 0 \end{pmatrix} \delta_1 + \begin{pmatrix} \bar{a}_2^p \\ 0 \\ \bar{a}_2^p \\ 0 \end{pmatrix} \begin{pmatrix} 0 & 1 & 0 \end{pmatrix} \delta_2 + \begin{pmatrix} 0 \\ \bar{a}_3^p \\ 0 \\ 0 \end{pmatrix} \begin{pmatrix} 1 & 0 & 0 \end{pmatrix} \delta_3 + \begin{pmatrix} 0 \\ \bar{a}_4^p \\ 0 \\ 0 \end{pmatrix} \begin{pmatrix} 0 & 1 & 0 \end{pmatrix} \delta_4 + \begin{pmatrix} \bar{b}_1^p \\ 0 \\ \bar{b}_1^p \\ 0 \end{pmatrix} \begin{pmatrix} 0 & 0 & 1 \end{pmatrix} \delta_5 + \begin{pmatrix} 0 \\ \bar{b}_2^p \\ 0 \\ 0 \end{pmatrix} \begin{pmatrix} 0 & 0 & 1 \end{pmatrix} \delta_6 \tag{37}$$

The MIMO framework for the analysis of the dynamic acceleration autopilot is formed in (38).

$$\begin{pmatrix} \dot{w} \\ \dot{q} \\ a_z \\ q \\ z_1 \\ z_2 \\ z_3 \\ z_4 \\ z_5 \\ z_6 \end{pmatrix} = \begin{pmatrix} \bar{a}_1^p & \bar{a}_2^p & \bar{b}_1^p & \bar{a}_1^p & \bar{a}_2^p & 0 & 0 & \bar{b}_1^p & 0 \\ \bar{a}_3^p & \bar{a}_4^p & \bar{b}_2^p & 0 & 0 & \bar{a}_3^p & \bar{a}_4^p & 0 & \bar{b}_2^p \\ \bar{a}_1^p & \bar{a}_2^p - u & \bar{b}_1^p & \bar{a}_1^p & \bar{a}_2^p & 0 & 0 & \bar{b}_1^p & 0 \\ 0 & 1 & 0 & 0 & 0 & 0 & 0 & 0 & 0 \\ 1 & 0 & 0 & 0 & 0 & 0 & 0 & 0 & 0 \\ 0 & 1 & 0 & 0 & 0 & 0 & 0 & 0 & 0 \\ 1 & 0 & 0 & 0 & 0 & 0 & 0 & 0 & 0 \\ 0 & 1 & 0 & 0 & 0 & 0 & 0 & 0 & 0 \\ 0 & 0 & 1 & 0 & 0 & 0 & 0 & 0 & 0 \\ 0 & 0 & 1 & 0 & 0 & 0 & 0 & 0 & 0 \end{pmatrix} \begin{pmatrix} w \\ q \\ \delta_e \\ w_1 \\ w_2 \\ w_3 \\ w_4 \\ w_5 \\ w_6 \end{pmatrix} \tag{38}$$

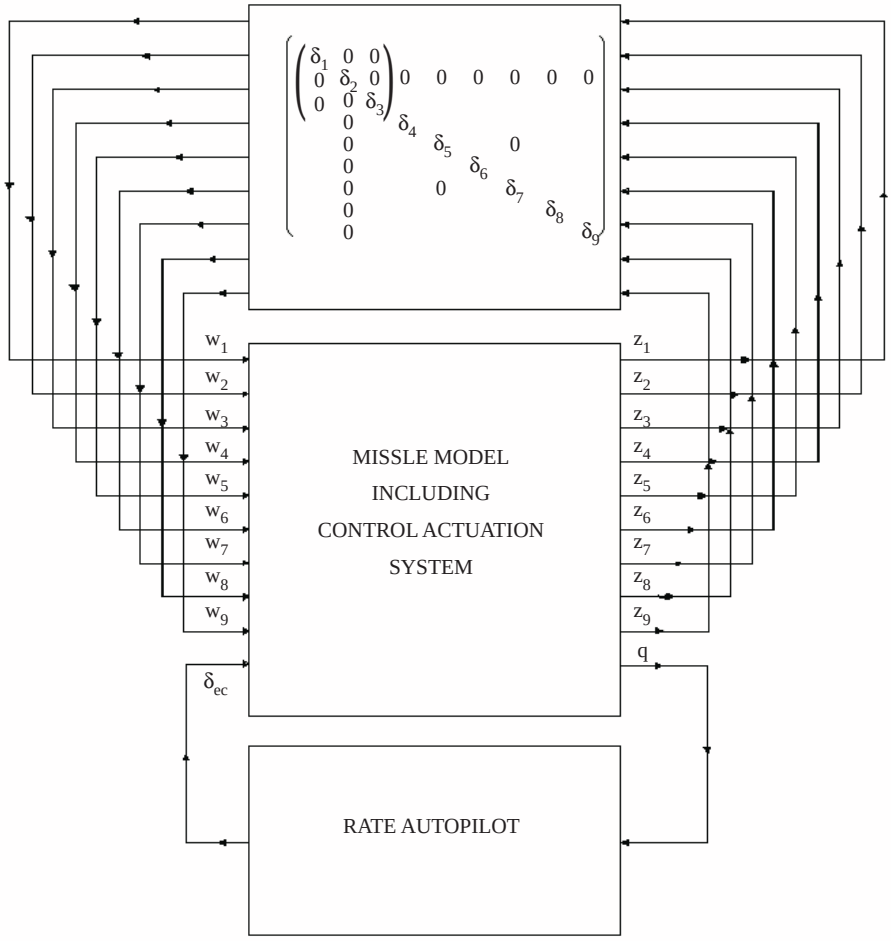

Figure 6. Complete linear fractional transformed form of the pitch rate autopilot.

The block diagram of the framework for the acceleration autopilot is shown in Figure 7. In both of the MIMO analysis equations in (34) and (38) there are some occurrences which can be thought as redundancies. General representation of those redundancies is the equivalency of output terms z_j as

$(z_1 = z_3,\ z_2 = z_4,\ z_5 = z_6)$. This is due to the effectiveness of two aerodynamic coefficients on each state variable and input $(w,\ q,\ \delta_e)$ of the pitch and yaw linear models in (7) and (8). The input – output pairs $(w_i,\ z_j)$ are not physical variables but they are the means of interaction of the uncertainty (Δ) to the physical nominal model aerodynamic coefficients of the missile.

3.2. Analysis and interpretation of the results

Analysis is performed for the nominally stable static and dynamic projective rate autopilots and the dynamic projective acceleration autopilot at each aerodynamic operating point (velocity and altitude). The algorithm of the MATLAB $\mu-$ analysis and synthesis toolbox [14] is used for the applications. For each operating point, the bounds of the structured singular value (upper bound μ_u and lower bound μ_l) for the closed loop linear autopilot is computed. The computation is performed by $\mu-$ algorithm at 200 frequency points in the range 10^{-3} to 10^4 radians per second. The algorithm of [9, 11, 12, and 14] can only compute the upper bound for the case of real parametric uncertainties. Although, this brings a degree of conservatism an acceptable level of upper bound may result in even a higher stability range.

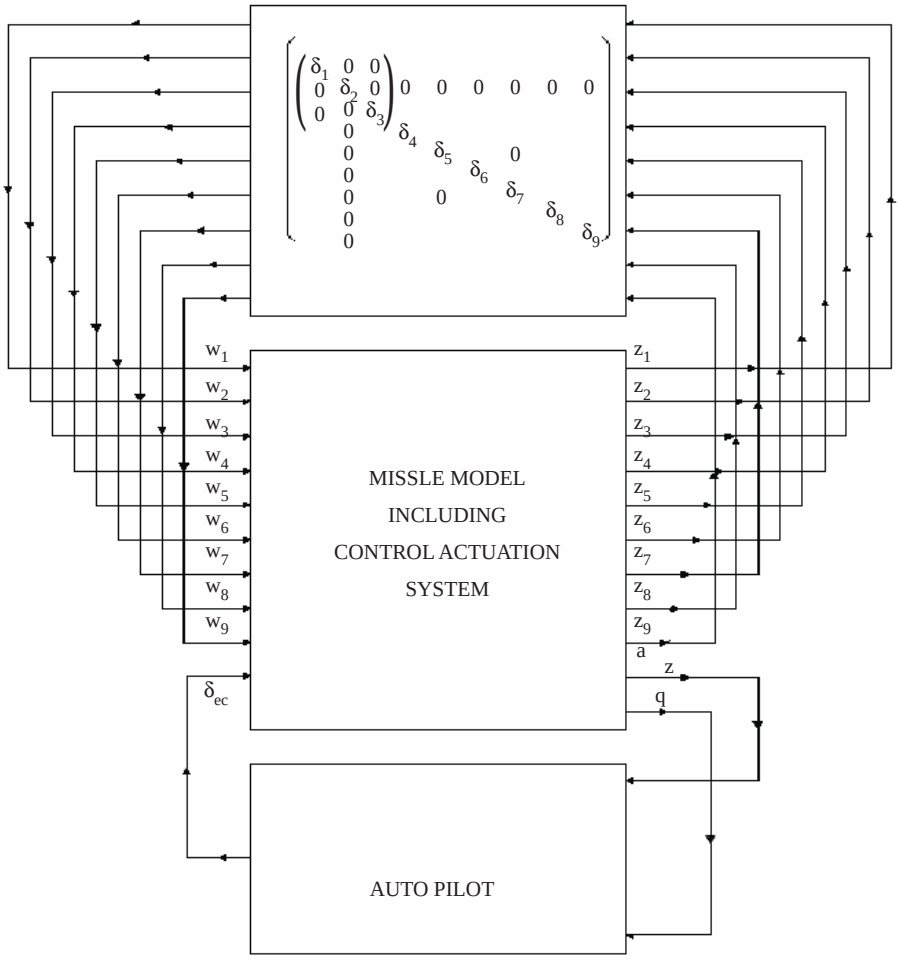

Figure 7. Complete linear fractional transformed form of the pitch acceleration autopilot.

The peak value of the upper bound $(\mu_u) -$ frequency distribution curve gives the most critical point $(\mu_{u\,c})$ for stability. This means that the closed loop system is stable for all parameter uncertainty sets (Δ_i)

which satisfy the following criterion:

$$\max_{\omega} \bar{\sigma} \left(\Delta \left(j\omega \right) \right) < \frac{1}{\mu_{u\,c}} \tag{39}$$

The value of $\mu_{u\,c}$ is taken as the result of the analysis for the relevant operating condition.

The variation of the reciprocal of the peak structured singular value (μ) with respect to the changing velocity and altitude are graphically expressed in Figure 8, Figure 9 and Figure 10 for static projective rate autopilot (SPRA), dynamic projective rate autopilot (DPRA) and dynamic projective acceleration autopilot (DPAA) respectively.

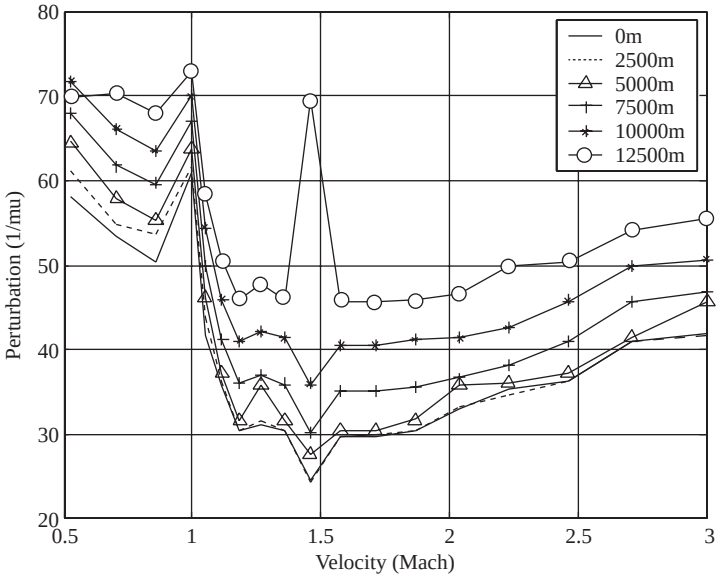

Figure 8. Variation of stability bound for static projective pitch rate autopilot.

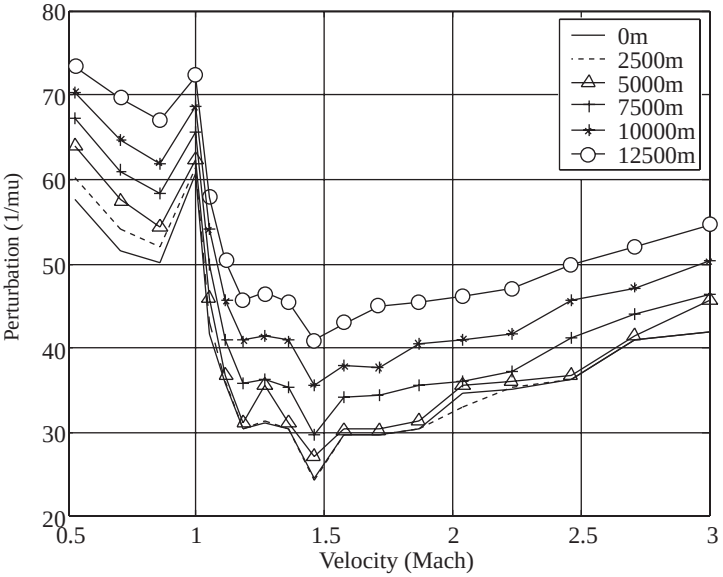

Figure 9. Variation of stability bound for dynamic projective pitch rate autopilot.

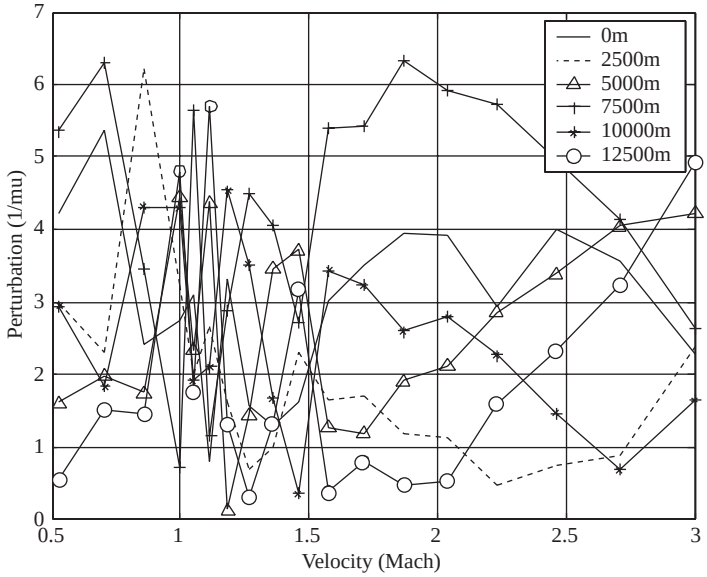

Figure 10. Variation of stability bound for dynamic projective pitch acceleration autopilot.

The variation of the robustness properties of the static and dynamic projective pitch rate autopilots with the aerodynamic operating points possess a minimum value at 25%. In real operation the aerodynamic coefficients C_i have a minimum of 15% uncertainty thus, the rate autopilots can operate successfully in real atmosphere. The robustness figures of dynamic projective acceleration autopilot are too far from applicable ranges as understood from Figure 10.

4. Real Environment Simulations

In structured singular value analysis, the stability issues related to aerodynamic and actuator related uncertainties are investigated. However in actual operation there are important external effects which should be taken into account. In real applications, the following disturbances have importance in flight performance considerations:

1. Aerodynamic parameter uncertainties: A minimum deviation of $\pm 15\%$ in aerodynamic coefficients is assumed.

2. Inertial Sensor Noise: The noise on turn rate and acceleration measurements is taken into account. These are modeled as zero mean normally distributed additive noise on variables $[p, q, r, a_x, a_y, a_z]$.

3. Thrust Misalignment: The misalignment in the orientation of the thrust force vector is an additive disturbance on aerodynamic forces and moments. It is defined by two normally distributed random angles [1].

4. Misalignment in the center of gravity: Mass production may lead to discrepancies in the position of the center of gravity for each manufactured missile body. Its effect is modeled as an additive normally distributed uncertainty on the position of center of gravity.

5. Initial Rolling: After the release from aircraft the missile may have an initial rolling within a range of $\pm 5^\circ$.

6. Actuator natural frequency: This may have a small uncertainty in the range $\pm 10\%$.

7. Side wind effects: The wind affecting from the lateral direction to the missile body is an important disturbance in real applications and it affects the body velocities $[u, v, w]$ with an exponential profile as shown below:

$$\begin{pmatrix} V_{wx} \\ V_{wy} \\ V_{wz} \end{pmatrix} = (1 - e^{-K_{w0}z}) \begin{pmatrix} V_{wx}^0 \\ V_{wy}^0 \\ V_{wz}^0 \end{pmatrix}$$
$$\begin{pmatrix} u_w \\ v_w \\ w_w \end{pmatrix} = \begin{pmatrix} u \\ v \\ w \end{pmatrix} - \begin{pmatrix} V_{wx}c\theta c\psi + V_{wy}c\theta c\psi - V_{wz}s\theta \\ V_{wx}(s\phi s\theta c\psi - c\phi s\psi) + V_{wy}(s\phi s\theta s\psi + c\phi c\psi) + V_{wz}s\phi c\theta \\ V_{wx}(s\phi s\theta c\psi + s\phi s\psi) + V_{wy}(c\phi s\theta s\psi - s\phi s\psi) + V_{wz}c\phi c\theta \end{pmatrix} \tag{40}$$

where $\begin{pmatrix} V_{wx} & V_{wy} & V_{wz} \end{pmatrix}^T$ represents the wind velocity in three directions at the specified altitude, $\begin{pmatrix} V_{wx}^0 & V_{wy}^0 & V_{wz}^0 \end{pmatrix}^T$ represents the wind velocity in the ground level and $\begin{pmatrix} u_w & v_w & w_w \end{pmatrix}^T$ is the body velocities of the missile including the wind effects. The wind is effective on the values of angle of attack and sideslip due to the change of body velocities. In addition, the solutions of the nonlinear missile model equations use the body velocity vector including the effect of wind.

In the simulations, it is assumed that the missile is released from the aircraft with the following initial conditions:

$$\begin{aligned} V_0 &= 0.9\,Mach \\ h_0 &= 40000\,ft = 12192\,m \\ x_f &= 50000\,m \\ y_f &= 20000\,m \end{aligned} \tag{41}$$

The nonlinear simulations are performed for the static and dynamic projective rate autopilots only. As the stability properties of the dynamic projective acceleration autopilot is not enough for a real application it is not considered. The nonlinear simulation analyses are based on the following measurements:

1. Angle of attack and sideslip
2. Pitch and yaw control surface deflections.
3. Pitch and yaw rates

In Figure 11 and Figure 12 the results related to the nonlinear simulation of the missile with static and dynamic projective rate autopilots are presented, respectively. For each case the simulation is repeated 100 times in order to have reliable information.

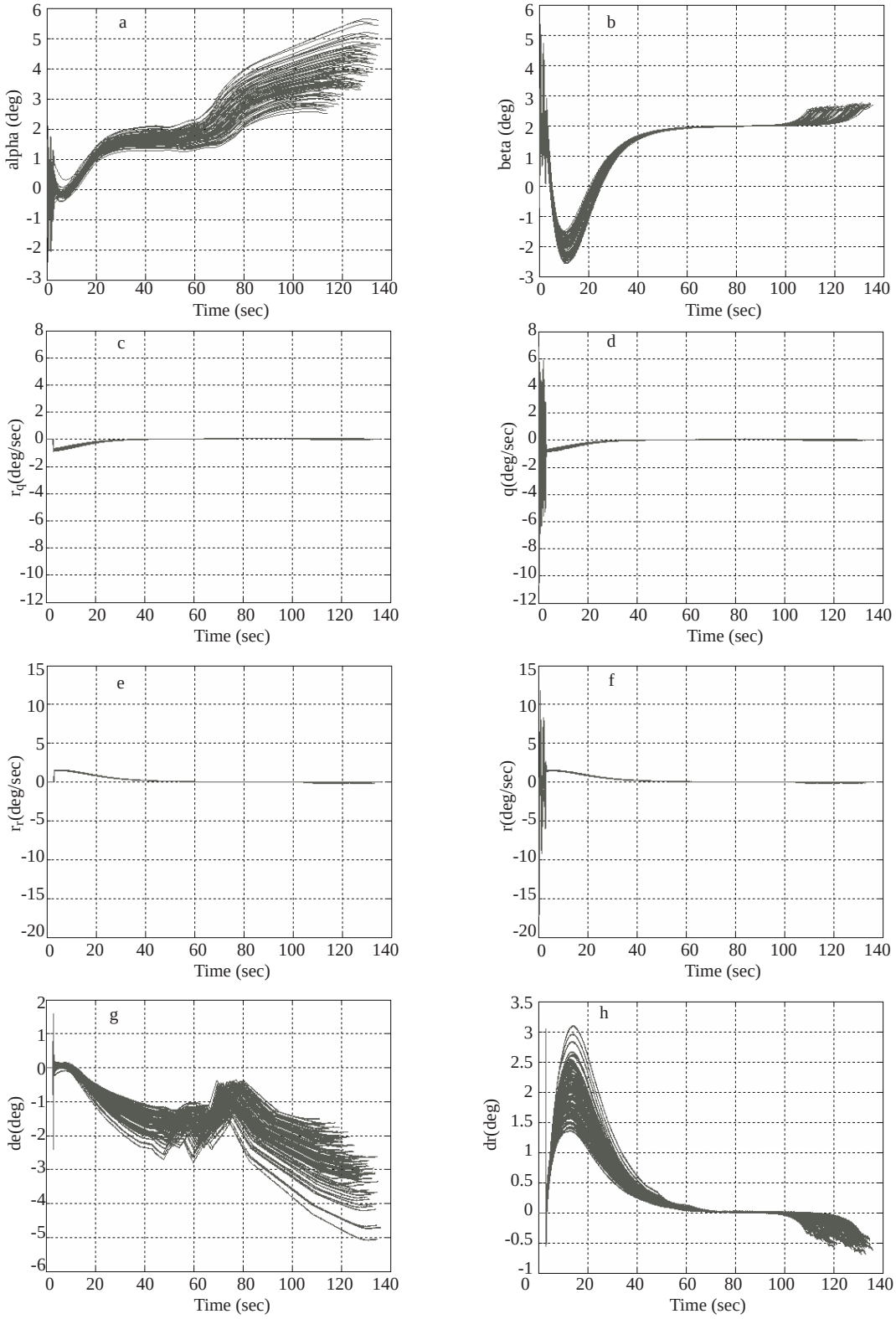

Figure 11. Variation of angle of attack and sideslip (a,b), pitch rate command and output (c,d), yaw rate command and output (e,f), pitch and yaw control surface deflections (g,h) for complete system having static projective pitch and yaw rate autopilots.

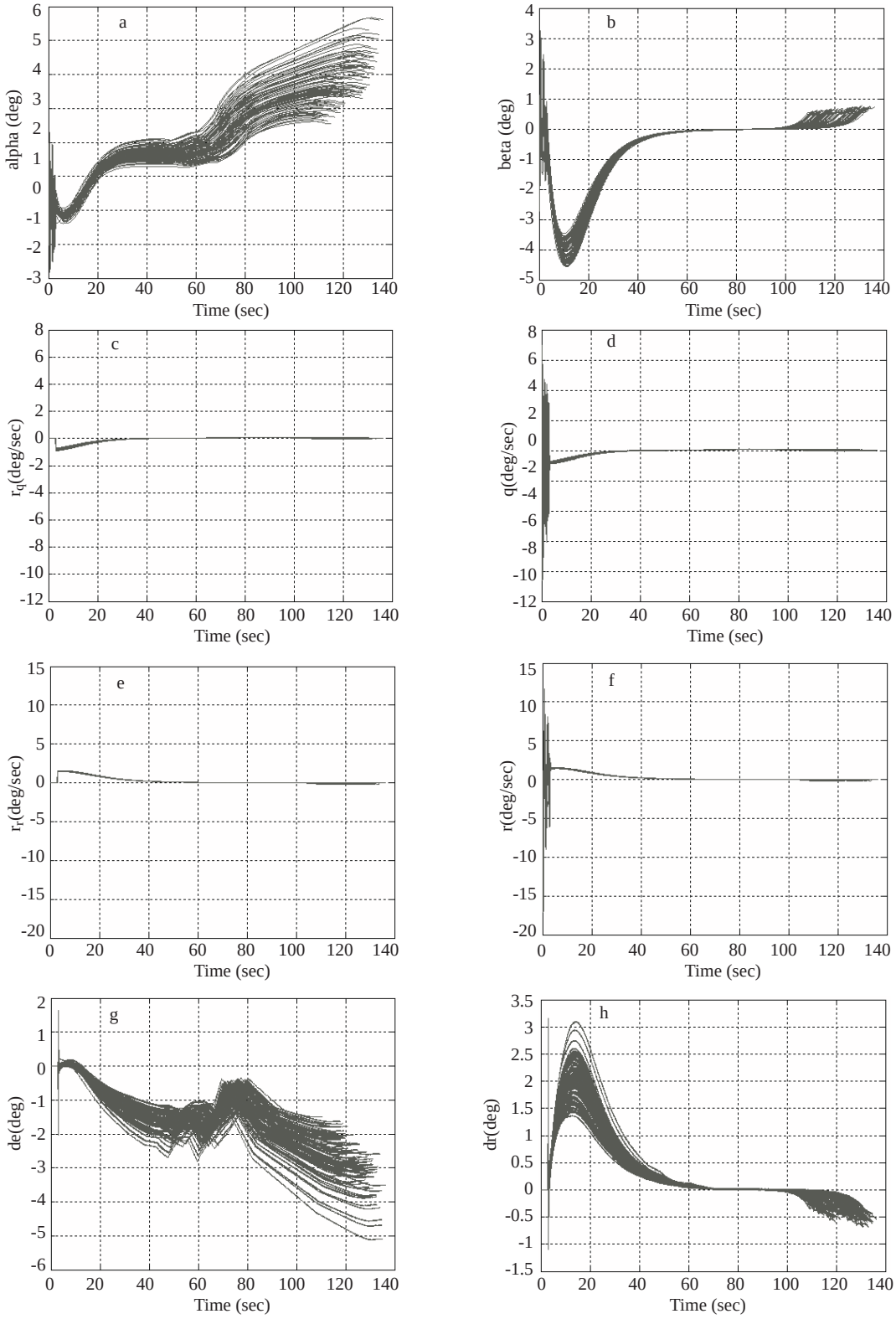

Figure 12. Variation of angle of attack and sideslip (a,b), pitch rate command and output (c,d), yaw rate command and output (e,f), pitch and yaw control surface deflections (g,h) for complete system having dynamic projective pitch and yaw rate autopilots.

5. Conclusion

In this paper, a complete robustness analysis for linear quadratic missile autopilots is presented. The application is performed on both pitch rate and acceleration autopilots. The projective control method itself is a practical tool for design automation purposes. However this research showed that it does not always guarantee an applicable design. The dynamic projective acceleration autopilot comes out to be inapplicable even it is nominally stable. The results of this research show that the differences in robustness properties of different autopilot designs are due to the model dependency of the linear quadratic theory. From one model to another, or even from one configuration to another, the performance and robustness may change considerably. The rate autopilots are successful in operation for a missile which has moderate dynamics and a stationary target. This result is also proven by real environment simulations. For new designs, a linear and after a nonlinear robustness analysis like in this research should be performed in order to obtain a wide range stable missile system.

References

[1] R.Ö. Doruk, "Missile autopilot design by projective control theory", M.Sc Thesis, Middle East Technical University, Electrical and Electronics Engineering Department, 2003.

[2] K.A. Wise, "Approximating a linear quadratic missile autopilot design using an output feedback projective control", AIAA Guidance, Navigation and Control Conference, Vol. 91 – 2613, pp. 114 – 122, 1991.

[3] J. Medanic, D. Petranovic, N. Gluhajic, "The design of output regulators for discrete – time linear systems by projective controls", International Journal of Control, Vol. 41, pp. 615 – 639, 1985.

[4] J. Medanic, Z. Uskokovic, "The design of optimal output regulators for linear multivariable systems with constant disturbances", International Journal of Control, Vol.37, pp.809 – 830, 1983.

[5] J.H. Blackelock, Automatic Control of Aircraft and Missiles, Prentice Hall, 1991.

[6] O. Atesoglu, "Design of different autopilot and their performance comparison", M.Sc Thesis, Middle East Technical University, Aerospace Engineering Department, 1997.

[7] D. McLean, Automatic Flight Control Systems, Prentice Hall, 1990.

[8] F.L. Lewis, B.L. Stevens, Aircraft Control and Simulation, New York Wiley, 1992.

[9] A. Packard, J.C. Doyle, "The complex structured singular value", Automatica Vol. 28, pp.71 – 109, 1993.

[10] K. Zhou, J.C. Doyle, Essentials of Robust Control, Prentice Hall, 1998.

[11] M. Fan, A. Tits, J.C. Doyle, "Robustness in the presence of mixed uncertainty and unmodeled dynamics", IEEE Transactions of Automatic Control Vol.36, pp.25 – 38, 1991.

[12] A. Packard, J.C. Doyle, "Structured singular value with repeated blocks", Proceedings of the American Control Conference Atlanta, pp.1213 – 1218, 1998.

[13] K.A. Wise, "Comparison of six robustness tests evaluating missile autopilot robustness to uncertain aerodynamics", AIAA Journal of Guidance, Control and Dynamics, Vol.15, pp.861 – 870, 1992.

[14] G.J. Balas, J.C. Doyle, K. Glover, A. Packard, R. Smith, MATLAB μ -Analysis and Synthesis Toolbox Version 3, Mathworks Inc., 1998.